Inorganic Chemistry

Article

pubs.acs.org/IC

A Diferrous Dithiolate as a Model of the Elusive H_{ox}^{inact} State of the [FeFe] Hydrogenases: An Electrochemical and Theoretical Dissection of Its Redox Chemistry

Dounia Chouffai,[†] Jean-François Capon,[†] Luca De Gioia,[‡] François Y. Pétillon,[†] Philippe Schollhammer,[†] Jean Talarmin,*[,†] and Giuseppe Zampella*[,‡]

[†]UMR CNRS 6521 Chimie, Electrochimie Moléculaires et Chimie Analytique, Université de Bretagne Occidentale, UFR Sciences et Techniques, CS 93837, 29238 Brest-Cedex 3, France

[‡]Department of Biotechnology and Bioscience, University of Milano-Bicocca, Piazza della Scienza 2, 20126 Milan, Italy

Supporting Information

ABSTRACT: The reduction of the Fe(II)Fe(II) complex $[Fe_2(CO)_2\{P(OMe)_3\}_2(\kappa^2\text{-}I_{Me}\text{-}CH_2\text{-}I_{Me})(\mu\text{-}CO)(\mu\text{-}pdt)]^{2+}$ ($\mathbf{2P^{2+}}$; pdt = $S(CH_2)_3S$), which is a synthetic model of the H cluster of the [FeFe] hydrogenases in its inactive state, has been investigated electrochemically and theoretically (by density functional theory, DFT) in order to determine the mechanisms, intermediates, and products of the related processes. The electrochemical reduction of $\mathbf{2P^{2+}}$ occurs according to an ECE-type reaction where the intervening chemical step is the loss of one $P(OMe)_3$ ligand. This outcome, which is based on cyclic voltammetric experiments, is strongly supported by DFT calculations that provide additional information on the intermediates and the energetics of the reactions involved. The electrochemical reoxidation of the neutral product of the reduction follows an EEC process where the chemical step is the binding of $P(OMe)_3$ to a dicationic intermediate. DFT calculations reveal that this intermediate has an unusual geometry wherein one of the two C−H bonds of a side methylene from the pdt group forms an agostic interaction with one Fe center. This interaction is crucial to stabilize the $32e^-$ diferrous center and concomitantly to preserve Fe(II) from binding of weakly coordinating species. Nonetheless, it could be displaced by a relatively stronger electron donor such as H_2, which could be relevant for the design of new oxidation catalysts.

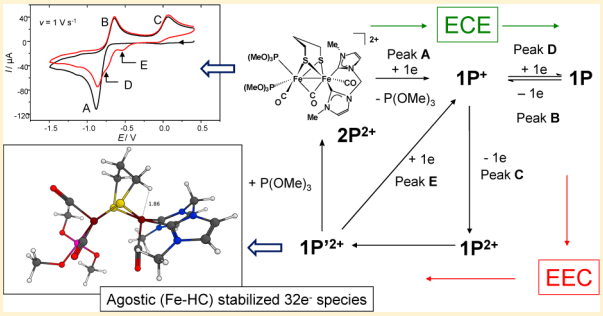

1. INTRODUCTION

Since the structure of the active site of the [FeFe] hydrogenases has been revealed,[1,2] numerous studies of this particular site, the so-called H cluster, have been reported.[3] The most studied states of the H cluster, that is, H_{ox}, H_{red}, and H_{sred}, are components of the enzymatic proton reduction/dihydrogen oxidation cycle, whereas the H_{ox}^{inact} (or H_{ox}^{air}) state (Scheme 1, left) is catalytically inactive.[3−9] Although some controversy exists regarding the number of electrons that are needed to reduce H_{ox}^{inact} to H_{ox},[3,6,9] the diiron subsite of the former is generally assigned an Fe(II)Fe(II) redox state.

The organometallic nature of the biological site also stimulated a number of synthetic works and reports on the reactivity of hundreds of models of the biological diiron subsite in the active Fe(I)Fe(I) (H_{red}) and Fe(I)Fe(II) (H_{ox}) states that have been published in the past decade or so.[10−18] Fewer studies have been devoted to models of the Fe(II)Fe(II) inactive site (H_{ox}^{inact}).

Nevertheless, several diferrous complexes have been obtained,[16,20−22] but little was known about their electron-transfer chemistry[16,20d] until the recent description of the reduction of a synthesized analogue of H_{ox}^{inact}, where the apical site of one of the iron atoms is occupied by the oxygen of a pendant ligand.[22] A $[Fe_2(CO)_6(\mu\text{-adt})]$ compound with a hydroxide bound at an apical position of the diiron site in the Fe(II)Fe(II) redox state has also been recently proposed as an intermediate of the oxygen reduction reaction catalyzed by hexacarbonyl diiron azadithiolate models (adt = $(SCH_2)_2NR$, R = Me or C_6H_5Br).[23]

We previously reported the synthesis of complex $\mathbf{2P^{2+}}$ (Scheme 1, right), which has some of the characteristic features of H_{ox}^{inact}, that is, an Fe(II)Fe(II) redox state, two terminal electron-releasing ligands, and one terminal CO bound to each iron atom, which are linked by bridging dithiolate and carbonyl ligands.[24] Complex $\mathbf{2P^{2+}}$ was obtained from neutral precursor $[Fe_2(CO)_4(\kappa^2\text{-}I_{Me}\text{-}CH_2\text{-}I_{Me})(\mu\text{-pdt})]$ (**1**, I_{Me} = 1-methylimidazol-2-ylidene) by chemical or electrochemical oxidation in the presence of $P(OMe)_3$, following a mechanism that involves the disproportionation of the cationic adduct ($\mathbf{1\text{-}P(OMe)_3^+}$, Scheme 2).[24]

Received: October 9, 2014
Published: December 12, 2014

   dx.doi.org/10.1021/ic5024746 | Inorg. Chem. 2015, 54, 299−311

Scheme 1. Schematic Representations of the Inactive Form of the [FeFe] Hydrogenases H Cluster[19] and of the $2P^{2+}$ Synthetic Model

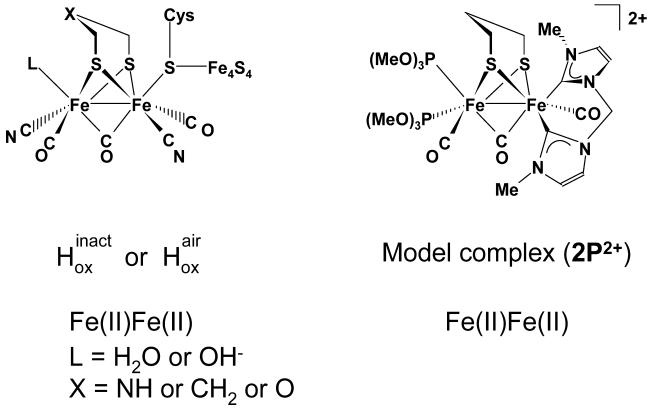

H_{ox}^{inact} or H_{ox}^{air} Model complex ($2P^{2+}$)

Fe(II)Fe(II) Fe(II)Fe(II)

L = H_2O or OH^-

X = NH or CH_2 or O

We now present the study of the electrochemical reduction of $2P^{2+}$ and the reoxidation of the reduced product as well as a detailed theoretical analysis of the mechanisms, intermediates, and products of the electron-transfer and chemical steps involved in these processes.

2. RESULTS AND DISCUSSION

In the following sections, the chelating ligand, κ^2-LL, will represent the chelating biscarbene (LL = I_{Me}-CH_2-I_{Me}) unless otherwise stated.

2.1. Electrochemical Study of the Reduction of $[Fe_2(CO)_2\{P(OMe)_3\}_2(\kappa^2\text{-LL})(\mu\text{-CO})(\mu\text{-pdt})]^{2+}$ ($2P^{2+}$). The cyclic voltammetry (CV) of $2P^{2+}$ measured at a scan rate of v = 0.2 V s^{-1} in CH_2Cl_2-$[NBu_4][PF_6]$ shows a reduction at a potential (E_p^{red})[25] of −0.84 V as well as two oxidation processes on the reverse scan (Figure 1, peaks A, B, and C, respectively). Although reduction A and oxidation B may at first sight appear to be a quasi-reversible process, this is not the case. The reduction is completely irreversible at all scan rates used in this study ($0.05 \leq v \leq 20$ V s^{-1}), whereas oxidation peak B is a component of a reversible system (B/D) with $E_{1/2}$ = −0.7 V, as shown by the second negatively going scan in Figure 1 (red trace).

In contrast to the behavior expected for a diffusion-controlled process, the current function ($i_p/v^{1/2}C$, where C is the concentration of the complex) for the reduction of $2P^{2+}$ is markedly dependent on v at slow scan rates (Figure 2). The comparison with the current function for the reversible one-electron oxidation[24] of $[Fe_2(CO)_4(\kappa^2\text{-LL})(\mu\text{-pdt})]$ (**1**, Figure 2) confirms a change in the number of electrons involved in the reduction of $2P^{2+}$, depending on the time scale of the experiment. Indeed, the peak current ratio $i_p^{red}(2P^{2+})/i_p^{ox}(1)$ decreases from 1.5 to ca. 1.1 when the scan rate (v) is increased

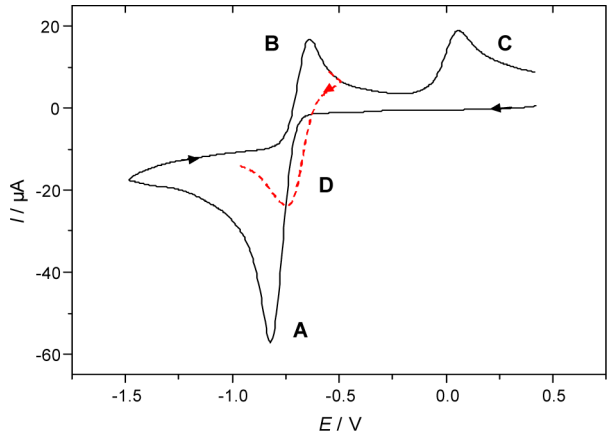

Figure 1. CV of $[Fe_2(CO)_2\{P(OMe)_3\}_2(\kappa^2\text{-LL})(\mu\text{-CO})(\mu\text{-pdt})]^{2+}$ ($2P^{2+}$, 1.8 mM) in CH_2Cl_2-$[NBu_4][PF_6]$ using a vitreous carbon electrode and a scan rate of v = 0.2 V s^{-1}; potentials are shown in volts (V) vs Fe^+/Fc.

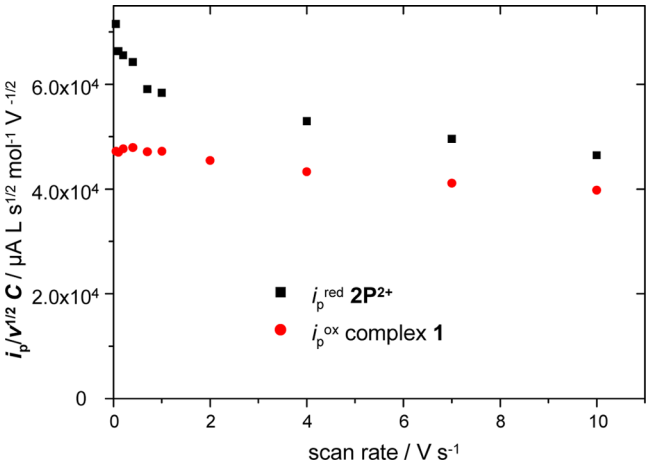

Figure 2. Scan rate dependence of the current functions ($i_p/v^{1/2}C$) for the reduction of $[Fe_2(CO)_2\{P(OMe)_3\}_2(\kappa^2\text{-LL})(\mu\text{-CO})(\mu\text{-pdt})]^{2+}$ ($2P^{2+}$, 1.75 mM, black square) and for the single-electron oxidation of $[Fe_2(CO)_4(\kappa^2\text{-LL})(\mu\text{-pdt})]$ (**1**, 1.78 mM, red ●) in CH_2Cl_2-$[NBu_4][PF_6]$.

from 0.05 to 10 V s^{-1} (Figure 2). This suggests that the reduction of $2P^{2+}$ involves an ECE-type mechanism at slow scan rates.[25,26] Thus, the primary reduction of $2P^{2+}$ to the undetected $\{2P^+\}$ at −0.84 V (Figure 1, peak A) is followed by a chemical step leading to a cation, which is reduced at the potential of peak D (Figure 1). The resulting neutral complex is characterized by an initial reversible single-electron oxidation at $E_{1/2}$ = −0.7 V (Figure 1, B/D system) and a second irreversible ($v \leq 20$ V s^{-1}) oxidation around 0.1 V (Figure 1, peak C). The potentials of the redox processes at peaks B/D and C are

Scheme 2

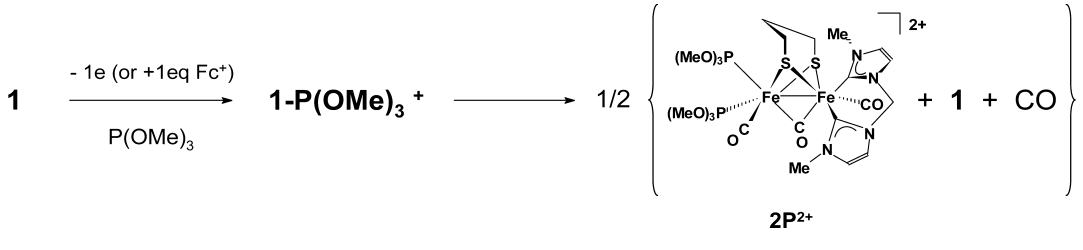

dx.doi.org/10.1021/ic5024746 | Inorg. Chem. 2015, 54, 299−311

consistent with those reported for $[Fe_2(CO)_3\{P(OMe)_3\}(\kappa^2\text{-dppe})(\mu\text{-pdt})]$ (dppe = $Ph_2PCH_2CH_2PPh_2$),[27] allowing for the shift in potential expected from the different electronic properties of the chelating ligands.[24,27] Therefore, we propose that the reaction following the first electron transfer is the loss of one $P(OMe)_3$ ligand from the undetected $\{\mathbf{2P}^+\}$. The resulting cation, $[Fe_2(CO)_3\{P(OMe)_3\}(\kappa^2\text{-LL})(\mu\text{-pdt})]^+$ ($\mathbf{1P}^+$), reduces reversibly at −0.7 V, which is the second electron transfer of the ECE process (Scheme 3).

Scheme 3. Proposed Mechanism for the ECE Reduction of $\mathbf{2P}^{2+}$ and the Reoxidation of $\mathbf{1P}$[a]

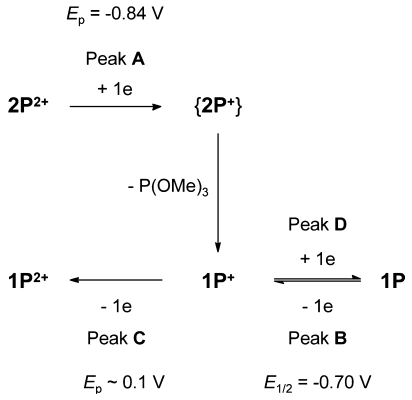

[a] $\{\mathbf{2P}^+\}$ was not detected.

The multiscan cyclic voltammetric experiments, carried out at different scan rates over a potential range encompassing peak A and the reversible B/D couple (Figure 3), show that the reduction of $\mathbf{2P}^{2+}$ remains irreversible at scan rates of up to v = 20 V s^{-1}, thus proving the intervening chemical reaction, assigned as the loss of one $P(OMe)_3$, to be fast. The presence of an isopotential point (IPP) at moderate to high scan rates ($v \geq 2$ V s^{-1}) indicates that two electroactive species are interconverting without any side reaction.[28−34] In the present case, this arises from the quantitative conversion of $\mathbf{2P}^{2+}$ into $\mathbf{1P}$, according to the ECE mechanism depicted in Scheme 3.

However, no IPP is present at slower scan rates (v = 0.2 V s^{-1}, Figure 3). This shows that a slower new reaction (prevented at faster scan rates) perturbs the interconversion of the electroactive species. The unidentified reaction observed at slow scan rates ($v \leq 0.2$ V s^{-1}) might be responsible for the failure of the controlled-potential electrolyses carried out at −0.9 V (peak A) to produce the desired complex ($\mathbf{1P}$). Instead, the voltammogram of the catholyte was completely different from the one expected from the CV run before electrolysis. The product resulting from the electrolysis was not characterized.

However, the $\mathbf{1P}^+/\mathbf{1P}$ couple can be confidently identified on the basis of the above results and those of the DFT calculations detailed below as $[Fe_2(CO)_3\{P(OMe)_3\}(\kappa^2\text{-LL})(\mu\text{-pdt})]^{+/0}$. Unlike the single-electron reduction of biological H_{ox}^{inact} to the Fe(I)Fe(II) site H_{ox},[6] $\mathbf{2P}^{2+}$ reduces directly to an Fe(I)Fe(I) species. This is also true for other synthesized Fe(II)Fe(II) models.[22,23]

2.2. Electrochemical Study of the Oxidation of $[Fe_2(CO)_3\{P(OMe)_3\}(\kappa^2\text{-LL})(\mu\text{-pdt})]$ (1P).

CV experiments were carried out in different potential ranges, in the absence or the presence of $P(OMe)_3$, to provide a deeper understanding of the chemistry associated with the reoxidation of $\mathbf{1P}$ on the CV time scale. When the second oxidation (peak C) is

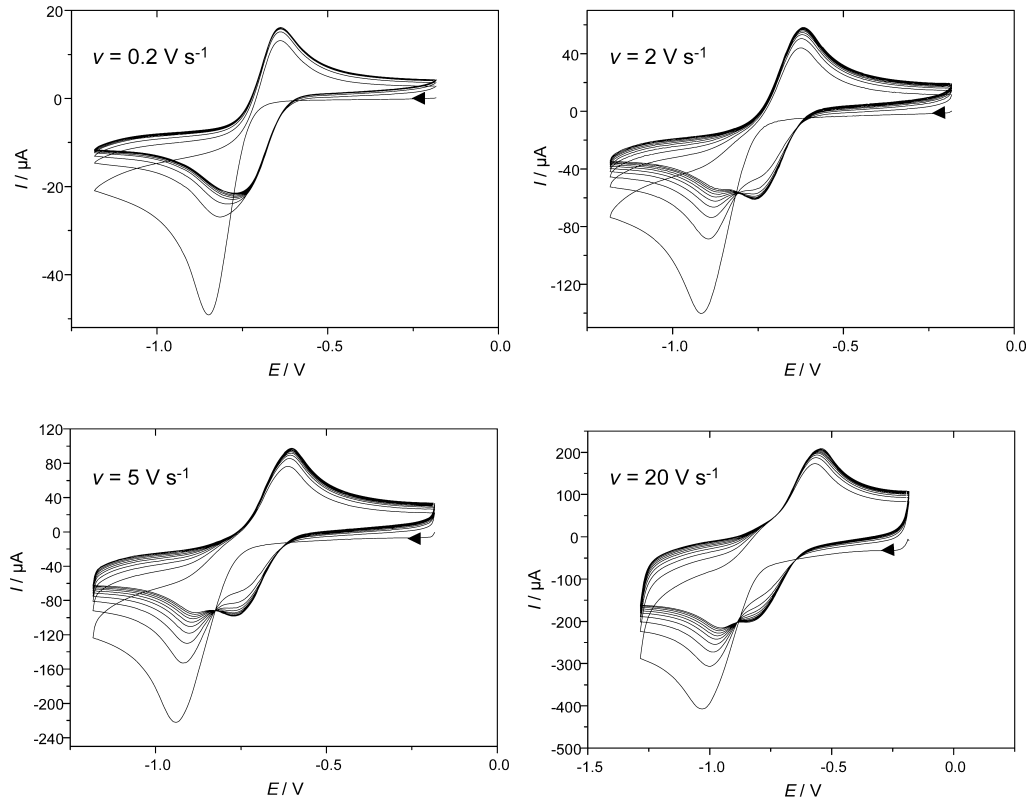

Figure 3. Repetitive CV (10 scans) of $[Fe_2(CO)_2\{P(OMe)_3\}_2(\kappa^2\text{-LL})(\mu\text{-CO})(\mu\text{-pdt})]^{2+}$ ($\mathbf{2P}^{2+}$, 1.75 mM) in CH_2Cl-$[NBu_4][PF_6]$ at different scan rates using a vitreous carbon electrode; potentials are shown in volts vs Fc^+/Fc.

dx.doi.org/10.1021/ic5024746 | Inorg. Chem. 2015, 54, 299−311

traversed, starting material $\mathbf{2P}^{2+}$ is regenerated, at least in a small amount (Figure S1). The addition of $P(OMe)_3$ to the solution enhances the regeneration of $\mathbf{2P}^{2+}$ significantly, as shown by the increased current of peak A relative to peak D under these conditions (Figure 4; black and green traces, respectively), which is indirect evidence that $P(OMe)_3$ loss occurred upon reduction of $\mathbf{2P}^{2+}$.

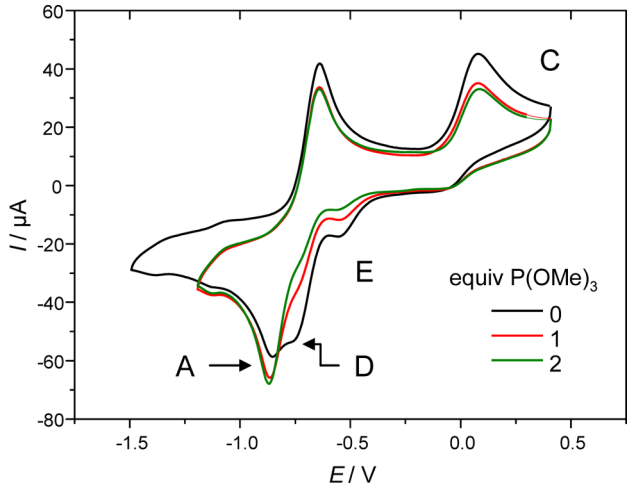

Figure 4. Steady-state (10th scan) CV of $[Fe_2(CO)_2\{P(OMe)_3\}_2(\kappa^2\text{-LL})(\mu\text{-CO})(\mu\text{-pdt})]^{2+}$ ($\mathbf{2P}^{2+}$, 1.8 mM) in the presence of various amounts of $P(OMe)_3$ in CH_2Cl_2-$[NBu_4][PF_6]$, using a vitreous carbon electrode and a scan rate of v = 1 V s^{-1}; potentials are shown in volts vs Fc^+/Fc.

Figure 4 also shows a noticeable decrease in reduction peak E upon addition of $P(OMe)_3$. This observation strongly suggests that the species reduced at peak E is a dication (Scheme 4, $\mathbf{1P'}^{2+}$) that reacts with trimethylphosphite to regenerate $\mathbf{2P}^{2+}$. The fact that peak C remains irreversible for scan rates of up to 20 V s^{-1} demonstrates that the dication initially arising from the oxidation of $\mathbf{1P}^+$ (that is, $\mathbf{1P}^{2+}$; Scheme 4) evolves to $\mathbf{1P'}^{2+}$ in a fast reaction. The different peaks observed in the CV data of $\mathbf{2P}^{2+}$ (Figure 5) can be identified as indicated in Scheme 4.

Aside from the different processes depicted in Scheme 4, homogeneous reactions involving electrogenerated species may occur, such as the disproportionation of cationic derivatives that

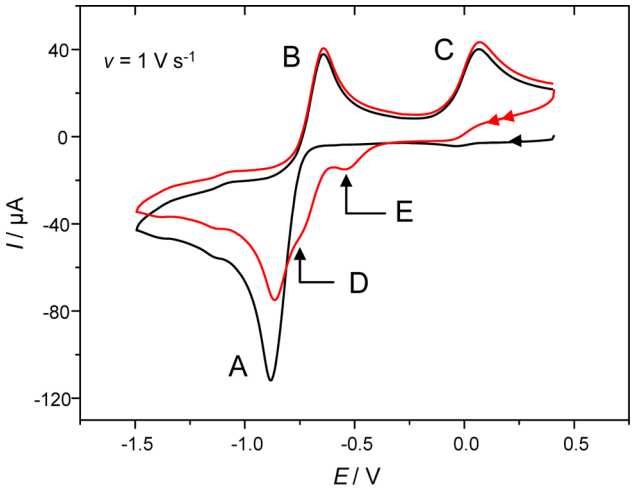

Figure 5. CV of $[Fe_2(CO)_2\{P(OMe)_3\}_2(\kappa^2\text{-LL})(\mu\text{-CO})(\mu\text{-pdt})]^{2+}$ ($\mathbf{2P}^{2+}$, 1.85 mM) in CH_2Cl_2-$[NBu_4][PF_6]$, showing the first and the second scans (black and red lines, respectively); the electrode processes occurring at the different peaks are shown in Scheme 4 (vitreous carbon electrode; potentials are in volts vs Fc^+/Fc).

was previously shown to contribute to the synthesis of $\mathbf{2P}^{2+}$ from $\mathbf{1}^+$ and $P(OMe)_3$.[24] In the present case, a homogeneous reaction may also contribute to the regeneration of $\mathbf{1P}^+$ on the CV time scale. Figure 5 illustrates that in spite of the complete irreversibility of the $\mathbf{1P}^+$ oxidation (peak C) and the small size of peak E on the reverse scan the amount of $\mathbf{1P}^+$ at the electrode is still important, as shown by the intensity of peak D. This feature was also met in the case of the oxidation of the diiron complexes $[Fe_2(CO)_4(\kappa^2\text{-LL})(\mu\text{-pdt})]$ (LL = I_{Me}-CH_2-I_{Me} (**1**);[24] dppe[27]) by two electrons; the small size of the reduction peak analogous to peak E was attributed to a homogeneous redox reaction of a rearranged dication with neutral compound **1**.[24] Similarly, we impute the intensity of peak D to the occurrence of reaction C2 (Table 1).

Digital simulations[35] of CV using different scan rates and two different potential ranges (covering the reduction of $\mathbf{2P}^{2+}$ and either the first or both oxidations of **1P**) were carried out according to a mechanism composed of the reactions in Table 1.[36] The CV data in Figures 6 and S2 show fair agreement

Scheme 4. Proposed Mechanisms for the Electrochemical Reduction of $\mathbf{2P}^{2+}$ and the Reoxidation of 1P

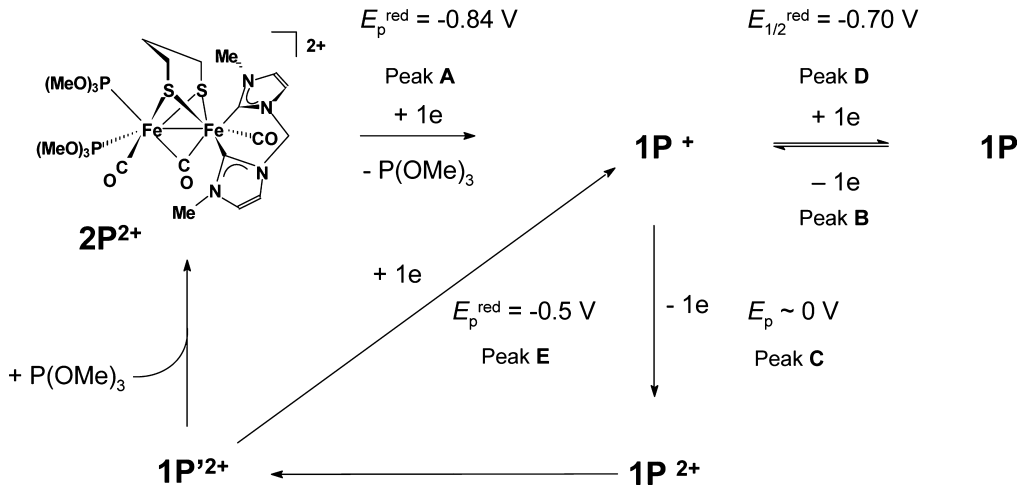

dx.doi.org/10.1021/ic5024746 | Inorg. Chem. 2015, 54, 299–311

Table 1. Steps Used for the Digital CV Simulations[35,36] and the Numerical Values of the Associated Constants

step[a]		E°/V	α	k_s/cm s^{-1}
R1	$\mathbf{1P^{2+}}$ + 1e = $\mathbf{1P^{+}}$	0	0.5	0.0015
R2	$\mathbf{1P^{+}}$ + 1e = **1P**	−0.68	0.5	0.01
R3	$\mathbf{2P^{2+}}$ +1e = $\mathbf{2P^{+}}$	−0.85	0.5	0.015
R4	$\mathbf{1P'^{2+}}$ + 1e = $\mathbf{1P'^{+}}$	−0.52	0.5	0.005
step[a]		K_{eq}	k_f	k_b
C1	$\mathbf{2P^{+}}$ = $\mathbf{1P^{+}}$ + P	10	800	80[b]
C2	$\mathbf{1P'^{2+}}$ + **1P** = $\mathbf{1P'^{+}}$ + $\mathbf{1P^{+}}$	505.9[b]	500	0.988[a]
C3	$\mathbf{1P'^{2+}}$ = $\mathbf{1P^{2+}}$	1000	1000	1[b]
C4	$\mathbf{1P'^{2+}}$ + P = $\mathbf{2P^{2+}}$	2.32×10^{10}[b]	200	8.6×10^{-9}[b]
C5	$\mathbf{1P^{2+}}$ + P = $\mathbf{2P^{2+}}$	2.32×10^{13}[b]	40	1.7×10^{-12}[b]
C6	$\mathbf{1P'^{+}}$ = $\mathbf{1P^{+}}$	6.14×10^{5}[b]	1000	0.0016[b]
C7	$\mathbf{2P^{2+}}$ + **1P** = $\mathbf{2P^{+}}$ + $\mathbf{1P^{+}}$	0.001 34[b]	3500	2.6×10^{6}[b]

[a]R = redox and C = chemical. [b]Calculated by DigiElch software.

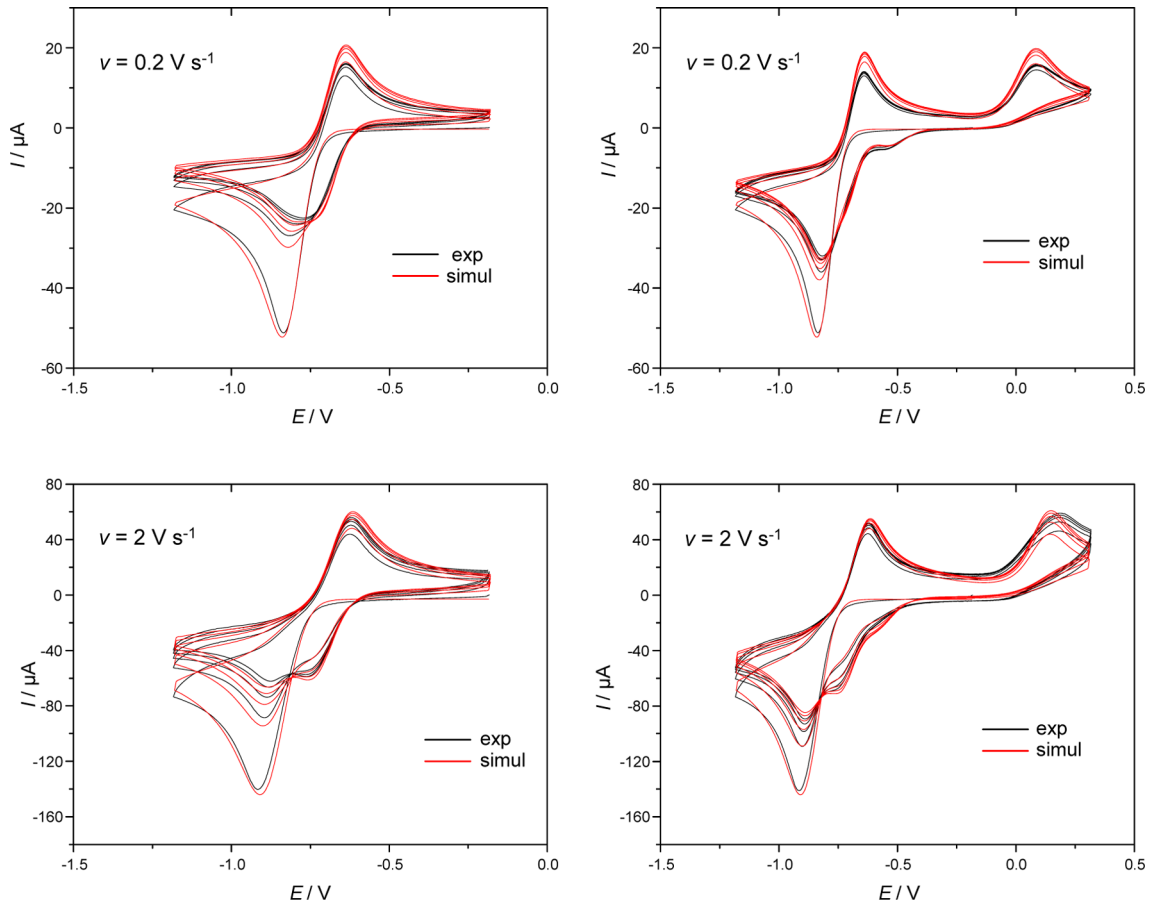

Figure 6. Experimental multiscan CV data of $[Fe_2(CO)_2\{P(OMe)_3\}_2(\kappa^2\text{-LL})(\mu\text{-CO})(\mu\text{-pdt})]^{2+}$ ($\mathbf{2P^{2+}}$, 1.75 mM) at v = 0.2 and 2 V s^{-1} in CH_2Cl_2-$[NBu_4][PF_6]$ (exp) and the digital simulations (simul) obtained using the parameters in Table 1.

between the experimental and the simulated data, which supports the mechanisms proposed in Scheme 4.

The study of the electrochemical behavior of the Fe(II)Fe(II) complex $\mathbf{2P^{2+}}$ showed that it is reduced following an ECE-type mechanism, whereas the Fe(I)Fe(I) reduction product **1P** oxidizes in a stepwise EEC process, making the Fe(I)Fe(II) oxidation step accessible. Because **1P** (and thus $\mathbf{1P^{+}}$) could not be obtained experimentally, a theoretical study was undertaken in order to obtain information about the nature of the products of the electrode and chemical processes as well as of the mechanisms and intermediates of the products' formation. To this end, we examined by density functional theory (DFT) the different steps of the mechanisms (Scheme 4) proposed on the basis of our experimental data. We first examined the consequences of the initial single-electron transfer and the relative stabilities of the possible cationic intermediates. Their absolute reduction potentials were compared to that of the parent dication in order to identify the actual molecular species that take part in the ECE process detected experimentally. The different possible neutral isomers were then examined in order to establish the nature of the final product of the reduction, **1P**. The stepwise oxidation of **1P** to $\mathbf{2P^{2+}}$ was also examined by DFT.

dx.doi.org/10.1021/ic5024746 | Inorg. Chem. 2015, 54, 299−311

2.3. Theoretical Study of the Primary Reduction of $2P^{2+}$ and of the Following Chemistry. DFT calculations carried out on the dicationic species show that the lowest unoccupied molecular orbital (LUMO) of $2P^{2+}$ has antibonding character along the Fe−$P(OMe)_3$ (apical) bond (Figure 7) so that the addition of the first electron is expected to induce the cleavage of this Fe−$P(OMe)_3$ bond.

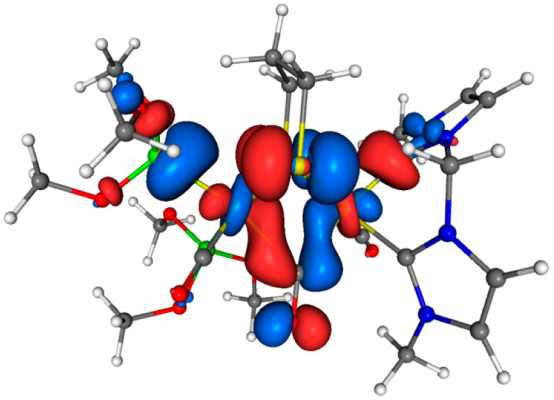

Figure 7. Representation of the LUMO of $2P^{2+}$. The cutoff value of the plotted isosurface is 0.05 a.u.

The DFT energy pathway associated with the loss of the apical $P(OMe)_3$ ligand clearly shows that $\{2P^+\}$ easily produces $[Fe_2(CO)_3\{P(OMe)_3\}(\kappa^2\text{-LL})(\mu\text{-pdt})]^+$, which is in agreement with the LUMO properties; the kinetic isomer of $[Fe_2(CO)_3\{P(OMe)_3\}(\kappa^2\text{-LL})(\mu\text{-pdt})]^+$ ($\mathbf{KI}^+$) is rotated[37] at the $Fe(CO)\{P(OMe)_3\}$ moiety (Scheme 5). Owing to the low energy barriers of the isomerization pathway (Scheme 6), $\mathbf{KI}^+$ is expected to rearrange very rapidly to the more stable form that is rotated at the $Fe(CO)(\kappa^2\text{-LL})$ center ($\mathbf{TI}^+$, Scheme 6).

The calculated reduction potential of $2P^{2+}$ (E = +4.62 V, −0.47 V vs Fc^+/Fc, Scheme 5) is significantly less negative than the experimental one (−0.85 V vs Fc^+/Fc, see above). This discrepancy is not surprising, in that it arises from piling up at least three different factors. The first one is the average error of 0.12 V, which is known to be associated with BP86 functional (generally affording the best performances) in reproducing experimental redox potentials.[38] The second source of error is due to the necessity of referencing computationally the absolute half-cell potential with respect to another electrode potential (Fc^+/Fc, in our case). BP86 values for the Fc^+/Fc reference have been reported to differ from the experimental value (0.65 V ± 0.01 V/SHE, determined in acetonitrile) by a value of up to 0.32 V.[39] Very recently, a strategy has been proposed that would avoid considering the reference electrode directly, thus circumventing errors associated with calculations of its potentials. This method requires, however, the availability of the redox potential of a third half-cell reaction (E°_{ref}) previously determined with respect to the same reference (for example, Fc^+/Fc) whose redox potential one does not want to calculate. Such a method is guaranteed to work only if a high similarity exists between the redox couple for which E°_{ref} is known and the couple under investigation.[40] However, in our case such a reference reaction was not available; furthermore, the exact reproduction of experimental values by theory was beyond the aim of this Article. Another source of error is due to the computing of the absolute redox potential of a dication/cation couple and then referencing it to that of a cation/neutral couple. This entails the deceptive prediction of the calculated potential of $2P^{2+} \rightarrow 2P^+$ reduction because of a limitation of the computational model, which is overly favored with respect to that of the reference (Fc^+/Fc). This shortcoming should be mitigated in principle by using explicit negative counterions, allowing for the normalization of the different charge effect of the two couples. Nonetheless, this strategy has been verified as only partially alleviating the problem (data not shown). Similar considerations of the theoretical versus experimental discrepancy regarding redox potentials can be found in the literature concerning combined DFT and electrochemical works.[41]

Given all that is discussed above, it is worth highlighting the role of DFT in the present investigation: DFT lends support in determining the kind of mechanism the electrochemical experiments are pointing to, in the sense that although our computed values are affected by imprecision they are still compatible with the ECE mechanism of reduction of $2P^{2+}$ proposed on an experimental basis.

Scheme 5. First Steps of the Reduction of $2P^{2+}$ Based on DFT Calculations

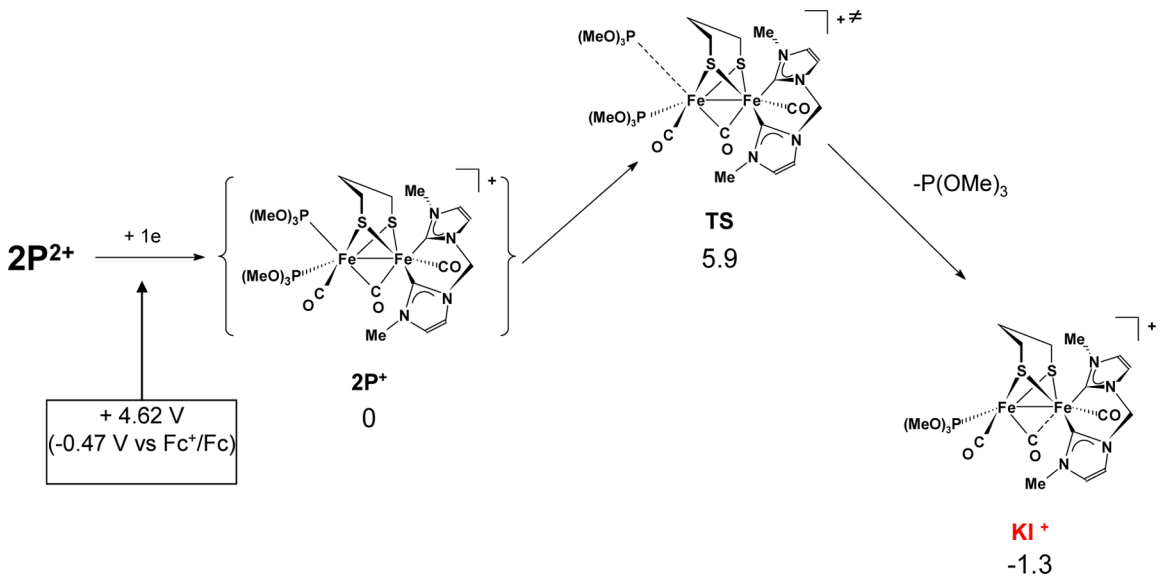

dx.doi.org/10.1021/ic5024746 | Inorg. Chem. 2015, 54, 299−311

Scheme 6. Isomerization of $[Fe_2(CO)_3\{P(OMe)_3\}(\kappa^2\text{-LL})(\mu\text{-pdt})]^{+a}$

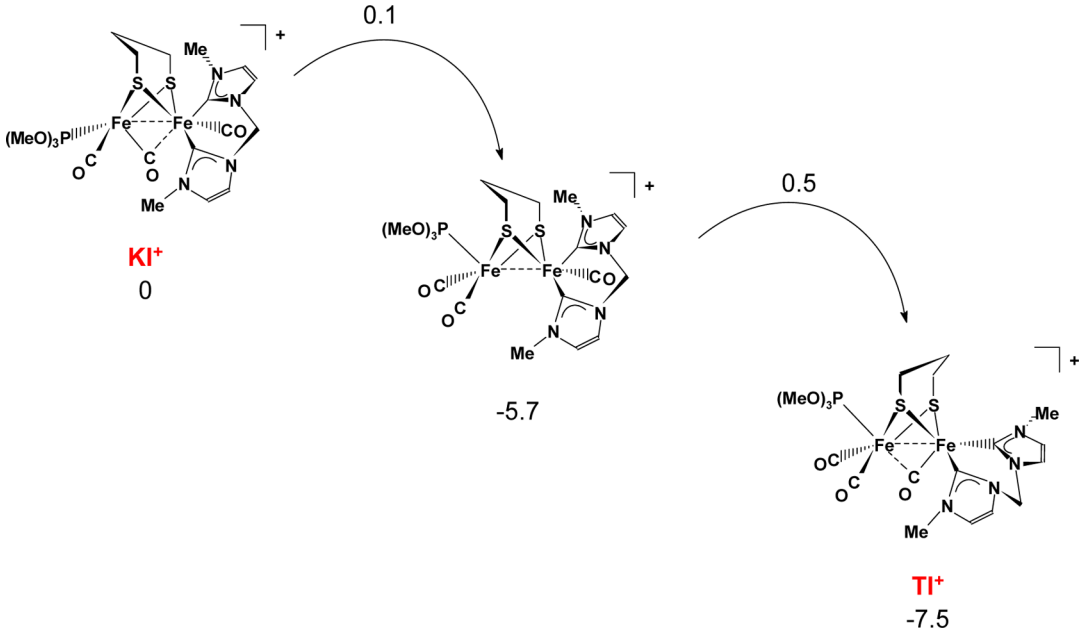

[a] $\mathbf{KI}^+$ and $\mathbf{TI}^+$ are the kinetic and thermodynamic isomers, respectively, of $[Fe_2(CO)_3\{P(OMe)_3\}(\kappa^2\text{-LL})(\mu\text{-pdt})]^+$. Curved arrows (instead of more typical straight lines) connecting intermediates and transition states emphasize the very fast evolution of $\mathbf{KI}^+$ to $\mathbf{TI}^+$.

Scheme 7. Possible Reactions Involved in the Two-Electron Reduction of $\mathbf{2P}^{2+a}$

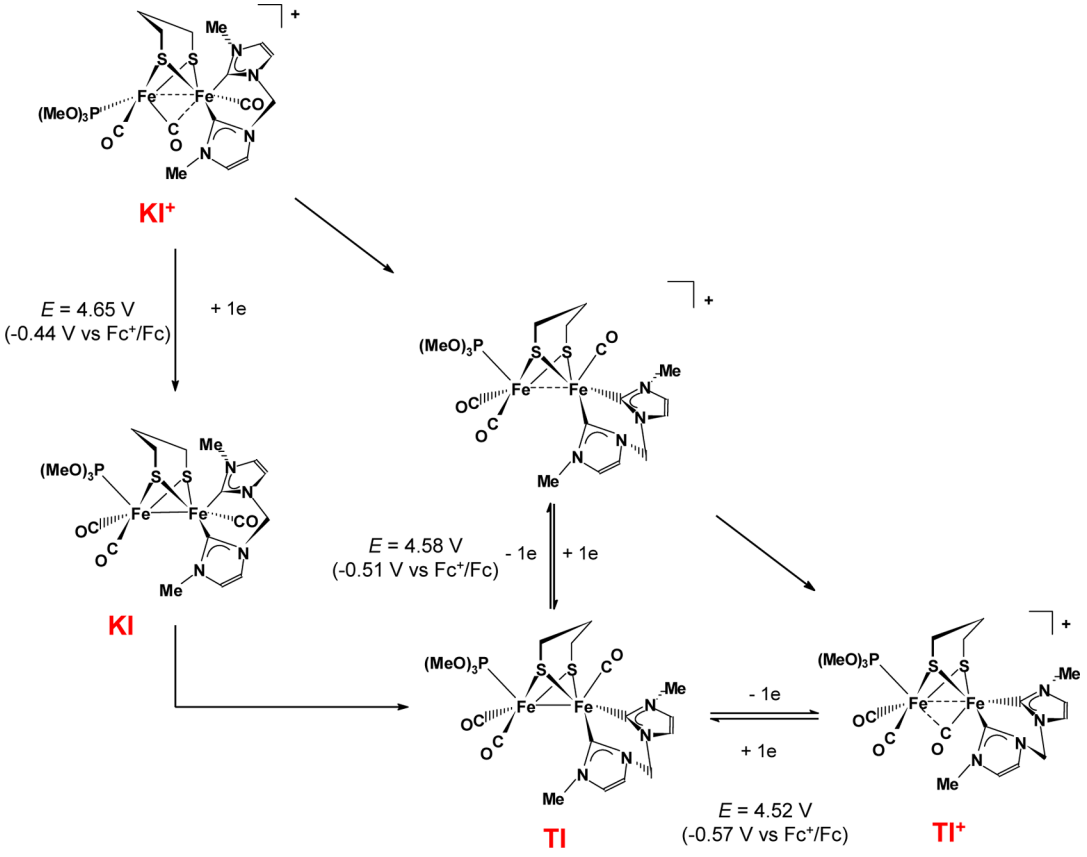

[a] Chemical (non-redox) steps, that is, diagonal and KI–TI pathways, are energy characterized in Schemes 6 and 8, respectively.

The calculated reduction potentials of both $\mathbf{KI}^+$ and $\mathbf{TI}^+$ show that $\mathbf{KI}^+$ is easier to reduce (E = +4.65 V; −0.44 V vs Fc^+/Fc) than $\mathbf{2P}^{2+}$, whereas the reduction of $\mathbf{TI}^+$ occurs at a potential that is 0.1 V more negative than that of $\mathbf{2P}^{2+}$ (Scheme 7). Specifically, the $\mathbf{TI}^+$ to **TI** reduction is predicted to occur at E = +4.52 V (−0.57 V vs Fc^+/Fc, Scheme 7). Therefore,

dx.doi.org/10.1021/ic5024746 | Inorg. Chem. 2015, 54, 299−311

Scheme 8. Energy Profiles Associated with the KI → TI Sequence Regarding Neutral Species Rearrangement[a]

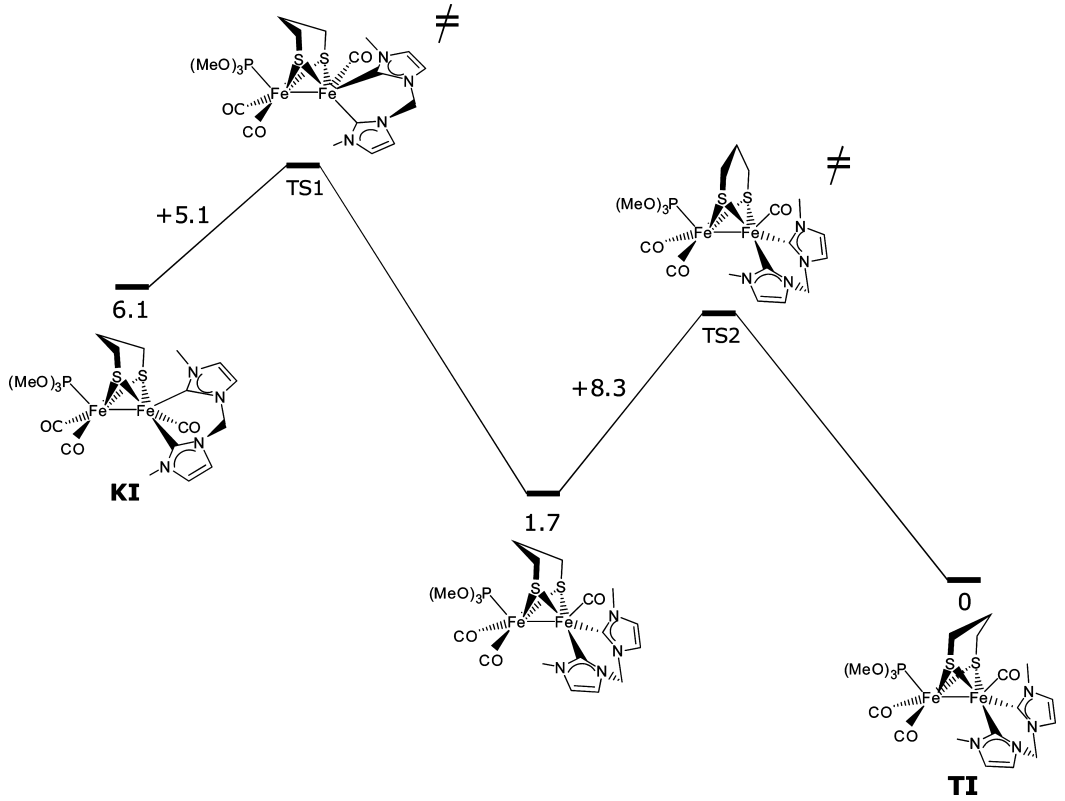

[a]Energy profiles are represented in kilocalories per mole (kcal mol^{-1}). Relative stabilities are indicated for DFT energy minima (**KI**, **TI**, and the 1.7 kcal mol^{-1} intermediate), whereas energy barriers are designated as "+*X*" with respect to the starting species in the **KI** → **TI** direction so that TS1 and TS2 are higher than **TI** (0) by 11.2 and 10.0 kcal/mol, respectively. TS1 is associated with rotation of Fe(NHC)(CO) group approximately about the Fe−Fe bond axis, whereas TS2 is associated with the pdt flip. The downhill energy profile and the computed low barriers are compatible with a process that is favored both thermodynamically and kinetically.

provided that the conversion of $\mathbf{2P}^{+}$ to $\mathbf{KI}^{+}$ (Scheme 5) is fast, $\mathbf{KI}^{+}$ is generated close to the electrode surface, where it is reduced to the neutral complex with an apical−basal coordination of the biscarbene ligand (**KI**, Scheme 7). This could represent, therefore, a possible mechanism for the second electron transfer of the ECE process detected by CV. Additionally, the almost barrierless $\mathbf{KI}^{+}$ → $\mathbf{TI}^{+}$ isomerization (Scheme 6) should also be fast so that the reduction of $\mathbf{2P}^{2+}$ might generate some cationic species with the $\mathbf{TI}^{+}$ geometry. Although the calculated reduction potential of $\mathbf{TI}^{+}$ is 0.1 V more negative than that of $\mathbf{2P}^{2+}$, we cannot exclude the possibility that the $\mathbf{TI}^{+}$/**TI** electron transfer contributes to the overall reduction process. Indeed, as previously mentioned, when comparing potentials of single-electron reductions of (or occurring at) differently charged systems, namely, a dication−cation ($\mathbf{2P}^{2+}$−$\mathbf{2P}^{+}$) versus a cation−neutral species ($\mathbf{TI}^{+}$−**TI**), it is expected that the deviations are significantly larger than those due to the intrinsic accuracy of the methodology. However, a difference of 0.1 V is already lower than such accuracy. Finally, an intermediate of the isomerization of $\mathbf{KI}^{+}$ to $\mathbf{TI}^{+}$ was identified (Scheme 7) and calculated to be reducible to **TI** at a potential of +4.58 V (−0.51 V vs Fc^{+}/Fc), which is quite close to the calculated reduction potential of $\mathbf{2P}^{2+}$. Therefore, this step might also be involved in the reduction process of the initial dication $\mathbf{2P}^{2+}$. Therefore, although $\mathbf{KI}^{+}$ can be confidently assimilated to $\mathbf{1P}^{+}$, $\mathbf{TI}^{+}$ and the intermediate between $\mathbf{KI}^{+}$ and $\mathbf{TI}^{+}$ (Scheme 7) might also represent the experimentally generated cation.

In light of the probable reduction of $\mathbf{KI}^{+}$ to **KI** near the electrode surface, dissection via DFT of the intimate mechanism of the **KI** → **TI** pathway has been made. In this case, the calculations point to a two-step process, as shown in Scheme 8.

A complete speciation by DFT of all of the possible forms of neutral complex $[Fe_2(CO)_3\{P(OMe)_3\}(\kappa^2\text{-LL})(\mu\text{-pdt})]$ demonstrates that the most stable isomer presents the chelating ligand in a dibasal arrangement (Scheme S1). This is a further indication that complex **1P** arising from the ECE-type mechanism (Schemes 3 and 4) is species **TI** presented in Schemes 7 and 8, thus **TI** = **1P**.

2.4. Theoretical Analysis of the Oxidation of $[Fe_2(CO)_3\{P(OMe)_3\}(\kappa^2\text{-LL})(\mu\text{-pdt})]$. Although the redox process with $E_{1/2}$ = −0.7 V looks quasi-reversible on the basis of the usual electrochemical criteria (peak separation, peak current ratio), **1P** and $\mathbf{1P}^{+}$ (Schemes 3 and 4) probably do not have the same geometry. Indeed, it is known that the single-electron oxidation of neutral diiron dithiolate complexes triggers a structure change that produces a cation with a rotated geometry.[15−18] Previous electrochemical studies of $[Fe_2(CO)_4(\kappa^2\text{-LL})(\mu\text{-pdt})]$ (LL = I_{Me}-CH_2-I_{Me} (**1**) or dppe) did not allow us to specify whether the rearrangement occurred in a stepwise (EC) or concerted (QR) fashion.[24,27] DFT calculations carried out on the oxidation of these compounds showed that the most stable cationic isomer is rotated at the $\{Fe_2(CO)(\kappa^2\text{-LL})\}$ center and is formed according to an EC process for LL = I_{Me}-CH_2-I_{Me}.[24]

dx.doi.org/10.1021/ic5024746 | *Inorg. Chem.* 2015, 54, 299−311

As expected from our previous studies and confirmed by a full speciation of cationic forms (Scheme S2 illustrates all of the isomers found), the calculated structure of the most stable cation, $\mathbf{TI}^{+}$, shows a rotated geometry at $\{Fe_2(CO)(\kappa^2\text{-LL})\}$, whereas **TI**, similar to nearly all of the other neutral Fe(I)Fe(I) complexes,[37] exhibits an eclipsed disposition (Schemes 7 and 8). It is thus tempting to draw a parallel between the experimental and theoretical results and to consider that **TI** = **1P**. DFT calculations for the oxidation of **TI** to $\mathbf{TI}^{+}$ indicate two possible routes: either an EC process passing through an eclipsed cation that is 1.4 kcal/mol higher in energy than $\mathbf{TI}^{+}$ or a concerted pathway where the electron transfer and the structure change are concomitant. These two possibilities are illustrated in Schemes 7 (bottom-right triangle) and S3.

From the DFT isomeric speciation carried out on the dicationic species likely to form upon oxidation of $\mathbf{TI}^{+}$, an unusual structure was identified that presents an agostic interaction between one metal center and a methylene proton of the pdt bridge (Figure 8; Scheme S4 reports relative stability

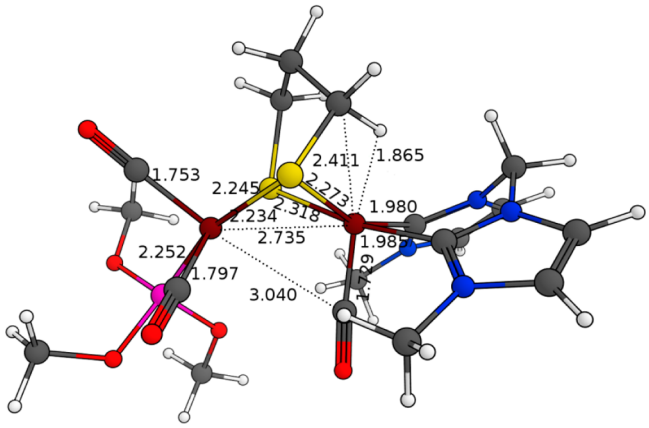

Figure 8. Representation of the DFT-optimized structure of the dication, showing an agostic interaction (angstroms) at the Fe(CO)-(κ^2-LL) center ($\mathbf{TI}^{2+}$). All relevant bonds and interatomic distances are shown in angstroms.

data for all isomers found). Although unusual, this kind of intramolecular interaction has already been speculated to form in other similar diferrous derivatives, provided that they did not present an amine as a dithiolate bridgehead (which has been proven to form an even more stable Fe(II)−NR_3 bond because it is a stronger electron donor than a C−H bond).[42] This agostic interaction cannot form with the central methylene group of pdt (Scheme S4).

This particular agostic dication, $\mathbf{TI}^{2+}$, might form via a precursor with the same geometry as $\mathbf{TI}^{+}$ (Scheme 9). $\mathbf{TI}^{2+}$ is likely to be the $\mathbf{1P'}^{2+}$ complex of Scheme 4. Indeed, the important structural difference between $\mathbf{TI}^{+}$ and agostic dication $\mathbf{TI}^{2+}$ might be the reason for the large potential separation between peaks C and E (Figure 5).

The above electron-transfer steps involving $\mathbf{TI}/\mathbf{TI}^{+}$ (Schemes 7 and S3) and $\mathbf{TI}^{+}/\mathbf{TI}^{2+}$ (Scheme 9) should be followed by a chemical reaction regenerating the starting dication $\mathbf{2P}^{2+}$ in order to complete the EEC process observed experimentally. Speciation by DFT of the possible isomers of dication $\mathbf{1P}^{2+}$ (Scheme S4) revealed the existence of another species 6.3 kcal/mol higher in energy than $\mathbf{TI}^{2+}$, showing an agostic interaction at the other iron center (Figure S3).

The energy barrier for the reaction of the second agostic dication (Scheme 10) with $P(OMe)_3$ was calculated to be 10.4 kcal/mol; thus, the global energy barrier for the reactions shown in Scheme 10 is at least 16.7 kcal/mol. The sequence in Scheme 10 is entirely consistent with the experimental results in that the limited regeneration of $\mathbf{2P}^{2+}$ observed by CV upon reoxidation of **1P** would arise from the $P(OMe)_3$-driven shift of an unfavorable equilibrium between the agostic dications.

Although peculiar (being formally a "two electron, three center" bond) and sometimes elusive with respect to full characterization (owing to the quite variable interatomic distances it can span), the agostic interaction found in $\mathbf{TI}^{2+}$ is compatible with recent observations concerning the same redox states of similar diiron dithiolates.[42,43] In fact, in both investigations the authors reported crystallographic structures of 32 e^- diferrous analogues of $\mathbf{TI}^{2+}$ (containing nitrogen-based dithiolate bridgeheads) in which the internal amine is coordinated to Fe(II). $\mathbf{TI}^{2+}$ has a pdt bridging the two Fe(II) ions, thus the electron density necessary to stabilize the unsaturated Fe(II) must come from the σ C−H bond of a methylene group. Two correlated structural features of diferrous derivatives presenting a nitrogen-containing S-to-S linker are the Fe_2S_2 core, changing its geometry from the typical butterflylike to a quasi-flattened (or nearly square-planar) one, and the Fe−Fe bond, which actually breaks upon oxidation of mixed valence Fe(II)Fe(I) species. In our case, owing to the weaker coordination of a C−H to Fe(II) compared to that of an amine, the Fe−Fe bond is strongly elongated and the butterfly core is only distorted. Notably, Zhang et al. have recently found that the same intramolecular agostic species is formed in a derivative strictly similar to $\mathbf{TI}^{2+}$ during the heterolytic activation of a $C(sp^3)$−H bond.[44] Furthermore, the authors indicated that the energetic accessibility of the agostic interaction is the crucial event making possible the full oxidation process (along with the presence of a suitable pendant nitrogen base).

Because of its peculiarity and its role in the stabilization of the Fe(II)Fe(II) state, we found the agostic interaction herein worthy of further investigation. Scheme 11 illustrates the DFT energetics of the binding process of PF_6^- (for example, coming from a large excess of supporting electrolyte) to the Fe(II) of $\mathbf{TI}^{2+}$ engaged in the agostic interaction with a methylene of pdt. This kind of calculation has been devised to test the stability of the agostic interaction in the presence of species endowed with even poor coordination properties (especially anions such as PF_6^-, but also CH_2Cl_2), which are present in great excess in the CV experiments. Because of its negative charge and the assumption of the weaker propensity of the neutral dichloromethane (vs anion) to bind the Fe(II) ion, only the energy profile for the addition of PF_6^- has been computed. Both in vacuo and in solvent simulations clearly show that the anion binding cannot displace the σ bond of methylene from Fe(II). Because entropic effects have also been estimated, we are able to conclude that these do not play any significant role in the observed result, the origin of which is therefore to be considered purely enthalpic. The strength of the HC−Fe interaction seems to lie in between that observed for the stronger N−Fe bond[42,43] and that originating from non-coordinating species. This observation could be useful as a device to exploit in the future for designing new H_2-activating catalysts. Indeed, overly stable covalent Fe(II)−NR_3 bonds cannot be displaced by incoming H_2, which conversely could more easily supersede a weaker agostic interaction. Of course,

dx.doi.org/10.1021/ic5024746 | Inorg. Chem. 2015, 54, 299−311

Scheme 9. Proposed Pathway of TI^{2+} Formation by the Oxidation of TI^{+} via a Transient Intermediate[a]

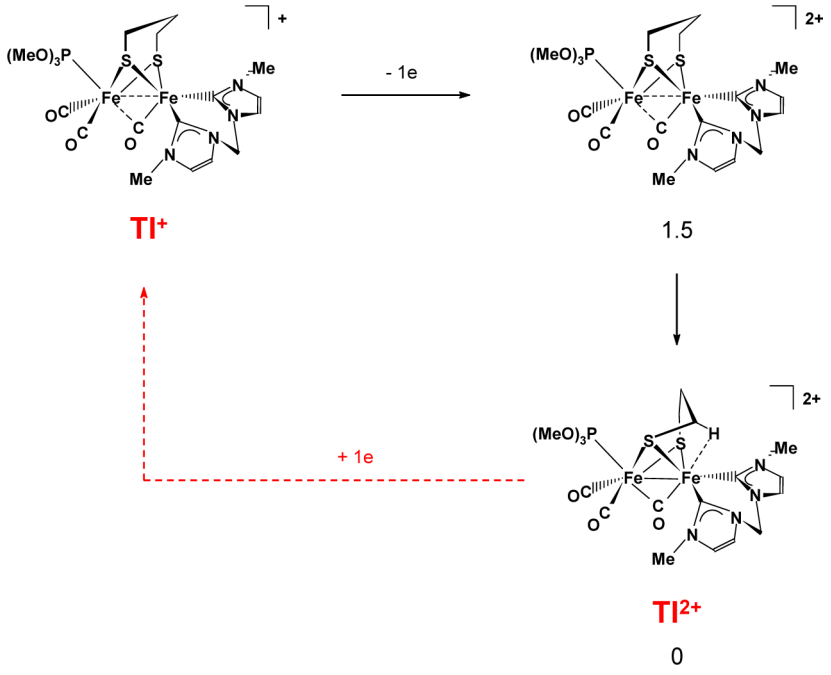

[a]Relative stability is displayed in kilocalories per mole for dication isomers.

Scheme 10. Proposed Pathway for the Regeneration of the Starting Dication via the Transient Formation of a Second Agostic Species[a]

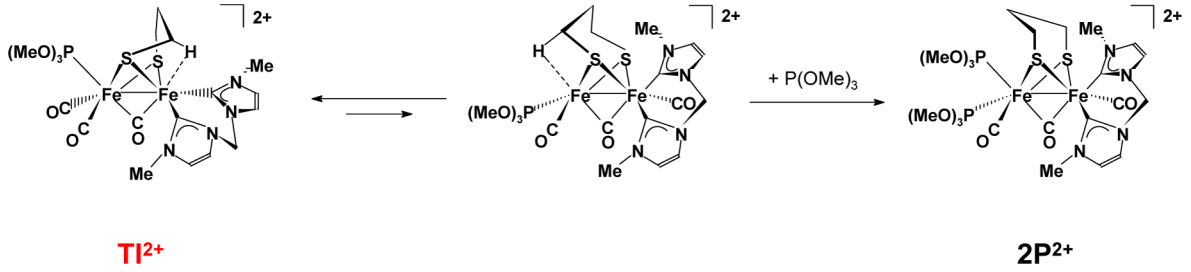

[a]Second agostic species is the middle species.

in order for such a system to function as heterolytic H_2-oxidation catalysts, the presence of either an inter- or an intramolecular base would be necessary in order to extract H^+ from H_2 without coordinating to Fe(II), owing to a properly tailored steric hindrance.[45] In such a case, the intramolecular agostic species has proven pivotal in the heterolytic activation of substrates other than H_2, that is, C(sp^3)−H-bond-containing derivatives.[44]

3. CONCLUSIONS

The work described in this Article may be summarized as follows. The electrochemical investigation of the reduction of diferrous complex $\mathbf{2P}^{2+}$ in dichloromethane shows that it occurs according to an ECE mechanism. The fast loss of a $P(OMe)_3$ ligand from the single-electron-reduced intermediate produces an Fe(I)Fe(II) cation that is easier to reduce than the parent dication. Thus, in contrast with the single-electron reduction of the Fe(II)Fe(II) $[2Fe]_H$ subsite of H_{ox}^{inact} to the Fe(I)Fe(II) diiron subsite of H_{ox}, the reduction of $\mathbf{2P}^{2+}$ leads directly to Fe(I)Fe(I) derivative **1P**.

DFT analysis of this process validates that the chemical step induced by the initial electron transfer is the loss of one $P(OMe)_3$ ligand from $\mathbf{2P}^{+}$, in that this process is both exergonic and fast. This chemical step leads to cation $[Fe_2(CO)_3\{P(OMe)_3\}(\kappa^2\text{-LL})(\mu\text{-pdt})]^+$ with a rotated $\{Fe_2(CO)P(OMe)_3\}$ moiety as the kinetic product ($\mathbf{KI}^+$). The reduction of $\mathbf{KI}^+$ occurs at a potential less negative than that of $\mathbf{2P}^{2+}$, which completes an ECE process in agreement with the cyclic voltammetric experiments. Concurrently, however, a fast conversion of $\mathbf{KI}^+$ to $\mathbf{TI}^+$ is strongly implied to occur on the basis of the low activation barriers involved in the isomerization. Nonetheless, although DFT predicts that $\mathbf{TI}^+$ is reduced at a potential ca. 0.1 V more negative than that of $\mathbf{2P}^{2+}$, we cannot rule out that the $\mathbf{TI}^+ \rightarrow \mathbf{TI}$ reduction contributes to the overall process because of the potential gap below the B-P86 intrinsic accuracy.

From the combined electrochemical and theoretical results, we conclude that **1P** = **TI**, whereas the conclusion concerning the identification of $\mathbf{1P}^+$ is less clear-cut. Indeed, on the basis of the DFT simulations, we cannot exclude the possibility that the single phosphine cation is either $\mathbf{TI}^+$ or $\mathbf{KI}^+$ (or even the intermediate between them, Scheme 7).

The electrochemical oxidation of **1P** to $\mathbf{2P}^{2+}$ follows an EEC process in which the second irreversible electron-transfer step is

dx.doi.org/10.1021/ic5024746 | Inorg. Chem. 2015, 54, 299−311

Scheme 11. ΔG (kcal/mol) of the Addition of a PF_6^- Anion to the Fe(II)-HC Site[a]

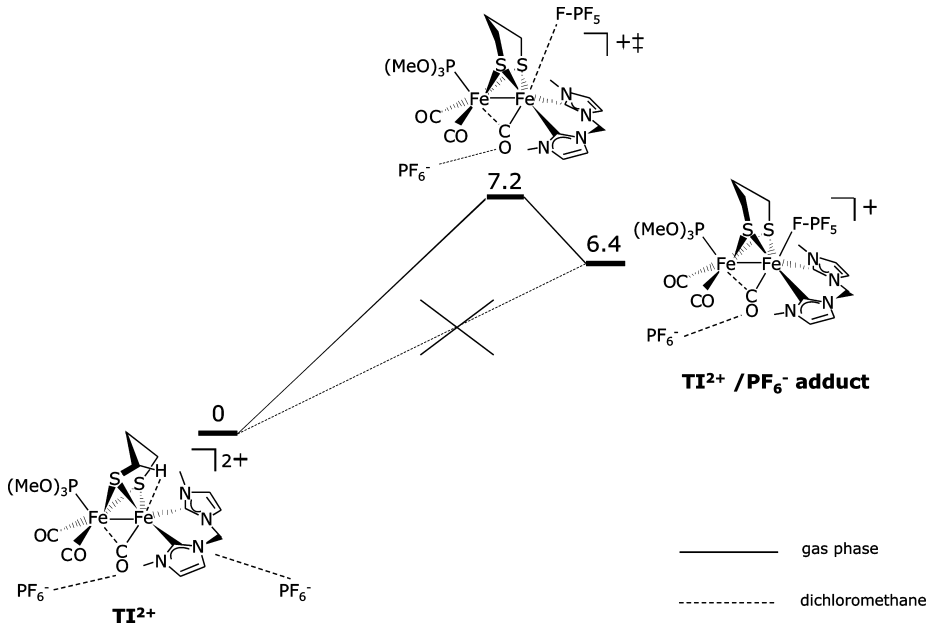

[a]When solvent presence is implicitly considered, the final adduct is not even an energy minimum on the potential energy surface of the [BP86/TZVP] level of theory.

likely coupled to a structure change. The DFT calculations are in full agreement with this outcome, revealing that the dicationic species, which is isostructural with the cationic precursor ($\mathbf{TI}^+$), rearranges to a distorted derivative showing an agostic interaction between a CH_2 σ bond from the pdt bridge and the iron center of the $\{Fe(I_{Me}\text{-}CH_2\text{-}I_{Me})\}$ fragment. Also, consistent with the experimental evidence that shows that the binding of $P(OMe)_3$ to the dicationic precursor of $\mathbf{2P}^{2+}$ is slow, DFT indicates that the regeneration of $\mathbf{2P}^{2+}$ requires an energy-costly structure change from $\mathbf{TI}^{2+}$ to an analogue where the agostic interaction occurs at the $\{Fe(CO)(P(OMe)_3)\}$ iron atom. The existence, although transient, of agostic diferrous intermediates could be exploited for the design of new mimics of [FeFe] hydrogenases, especially in the direction of H_2 activation.

4. EXPERIMENTAL SECTION

Reactions were carried out under nitrogen using standard Schlenck techniques. All reagents were used as purchased (Sigma-Aldrich). The solvents were predried using conventional methods and were distilled prior to use. Compounds $[Fe_2(CO)_4(\kappa^2\text{-LL})(\mu\text{-pdt})]$ (**1**) and $[Fe_2(CO)_2\{P(OMe)_3\}_2(\kappa^2\text{-LL})(\mu\text{-CO})(\mu\text{-pdt})]^{2+}$ ($\mathbf{2P}^{2+}$) were obtained following reported procedures.[24,46]

The preparation and the purification of the supporting electrolyte $[NBu_4][PF_6]$ were as described previously.[24] The electrochemical equipment consisted of a PGSTAT 12 or a μ-AUTOLAB (type III) driven by the GPES software. A GCU potentiostat and an IG5-N integrator (Tacussel/Radiometer) were used for controlled-potential electrolyses and coulometry. The working electrode consisted of a vitreous carbon disk that was polished on a felt tissue with alumina, rinsed with water, and dried before each CV scan. The Ag/Ag^+ reference electrode was separated from the analyte by a CH_2Cl_2-$[NBu_4][PF_6]$ bridge. All of the potentials (text, figures) are referenced to the ferrocene−ferrocenium couple; ferrocene was added as an internal standard at the end of the experiments.

4.1. Digital Simulations. All simulations were run using DigiElch Special Build Version 3 (Build SB3.600).[35] In addition to the numerical values in Table 1, the simulations were carried out with the same diffusion coefficient ($D_0 = 3.5 \times 10^{-6}$ cm^2 s^{-1}) for all the species and an electrode area A = 0.072 cm^2. The values of the uncompensated solution resistance and the double-layer capacitance were 80 Ω and 1.5×10^{-6} F, respectively.

5. COMPUTATIONAL METHODS

DFT calculations were carried out using the pure functional B-P86[47] and a valence triple-z basis set plus polarization on all atoms (TZVP).[48]

Calculations were made using TURBOMOLE code[49] together with the resolution-of-the-identity technique.[50] Stationary points on the energy hypersurface were located by means of energy-gradient techniques, and full vibrational analysis was carried out to characterize all stationary points found.

On the basis of the restricted second-order method adopting Hessian shift parameters, the transition-state structures were optimized according to a quasi-Newton−Josephson procedure.[51] (See also the manual of ref 49 and references therein.) First, geometry optimization of an estimate of the real transition-state structure is carried out by fixing the degree(s) of freedom that is (are) associated with the reaction coordinate. Second, vibrational analysis of the located minimum-energy structures is carried out. Third, if one negative eigenmode corresponding to the reaction coordinate is found, then the curvature determined at that point is employed to search for the true transition state. This last step entails the use of an eigenvector-following procedure: the eigenvectors in the Hessian are sorted in ascending order, with the first one being the eigenvector that corresponds to the negative eigenvalue. Subsequently, the search proceeds by choosing the critical eigenvector according to a maximum overlap criterion based on the inner product between the ith eigenvector and the $(i + 1)$th vector followed in the previous step. Then, the analytical Hessian is calculated to confirm the nature of the located stationary point, which must be a first-order saddle point on the investigated potential hypersurface.

Free-energy (G) corrections were made to the pure electronic SCF energy by evaluating the system partition function Q under the desired temperature and pressure conditions and by approximating Q as a product of all of those terms that contribute separately to its formation (translations, rotations, and vibrations).

Rotations were treated classically (rigid-rotor approximation), and vibrational modes were described according to the harmonic

dx.doi.org/10.1021/ic5024746 | Inorg. Chem. 2015, 54, 299−311

approximation. The ideal-gas assumption was also employed to transform the enthalpic relation $H = E + PV$ into the simpler form of $H = E + RT$.

The effect of the solvent (dichloromethane, $E = 9.1$) was evaluated according to the COSMO approach.[52]

Reduction potentials (in volts) were calculated according to eq 1, represented as

$$\Delta G^\circ = -nFE^\circ \quad (1)$$

in which n is the number of electrons transferred (in our case, $n = 1$), F is the Faraday constant (96 485.338 C mol^{-1}), and the ΔG° value is represented in joules per mole.

The resulting E° value is an absolute reduction potential; that is, it is not referenced to any standard electrode. Therefore, in order to obtain the reduction potential versus the Fc^+/Fc couple taken as a reference, the absolute reduction potential of 5.05 V (determined in CH_3CN)[53,54] was systematically subtracted from the E° value. A final correction of 0.04 V was applied to account for the approximate liquid junction potential of the acetonitrile/dichloromethane interface because of the solvent employed in the present study (CH_2Cl_2).[55] Therefore, the calculated E° (in volts) was obtained according to eq 2, represented as

$$E^\circ\,(\mathrm{V}) = \frac{\Delta G^\circ(\mathrm{J\ mol^{-1}})}{-1 \times F} - 5.09\ (\mathrm{V}) \quad (2)$$

The values of standard reduction potentials were computed by taking solvation contributions into account.

■ ASSOCIATED CONTENT

Supporting Information

Figures of multiscan cyclic voltammetry and digital simulations; figure of the DFT-optimized structure of the dication showing an agostic interaction at the $Fe(CO)\{P(OMe)_3\}_2$ center; diagrams showing the relative stabilities (kilocalories per mole) of isomers **1P**, $\mathbf{1P^+}$, and $\mathbf{1P^{2+}}$; and scheme showing the two routes for the oxidation of **TI** (= **1P**) to $\mathbf{TI^+}$ (= $\mathbf{1P^+}$) proposed from DFT calculations. This material is available free of charge via the Internet at http://pubs.acs.org.

■ AUTHOR INFORMATION

Corresponding Authors

*E-mail: jean.talarmin@univ-brest.fr.

*E-mail: giuseppe.zampella@unimib.it.

Notes

The authors declare no competing financial interests.

■ ACKNOWLEDGMENTS

Financial support was provided by CNRS (Centre National de la Recherche Scientifique), Université de Bretagne Occidentale, and University of Milano-Bicocca. The authors are grateful to Dr. M. Rudolph for providing the DigiElch software. D.C. thanks the Ministère de l'Education Nationale de l'Enseignement Supérieur et de la Recherche for providing a studentship. L.D.G. acknowledges support from MIUR (prin 2010M2JARJ).

■ REFERENCES

(1) (a) Peters, J. W.; Lanzilotta, W. N.; Lemon, B. J.; Seefeldt, L. C. *Science* **1998**, *282*, 1853−1858. (b) Lemon, B. J.; Peters, J. W. *Biochemistry* **1999**, *38*, 12969−12973.

(2) (a) Nicolet, Y.; Piras, C.; Legrand, P.; Hatchikian, C. E.; Fontecilla-Camps, J. C. *Structure* **1999**, *7*, 13−23. (b) Nicolet, Y.; de Lacey, A. L.; Vernede, X.; Fernandez, V. M.; Hatchikian, C. E.; Fontecilla-Camps, J. C. *J. Am. Chem. Soc.* **2001**, *123*, 1596−1602.

(3) For recent reviews on the hydrogenases enzymes, see: (a) Fontecilla-Camps, J. C.; Volbeda, A.; Cavazza, C.; Nicolet, Y. *Chem. Rev.* **2007**, *107*, 4273−4303. (b) de Lacey, A. L.; Fernandez, V. M.; Rousset, M.; Cammack, R. *Chem. Rev.* **2007**, *107*, 4304−4330. (c) Lubitz, W.; Reijerse, E.; van Gastel, M. *Chem. Rev.* **2007**, *107*, 4331−4365. (d) Vincent, K. A.; Parkin, A.; Armstrong, F. A. *Chem. Rev.* **2007**, *107*, 4366−4413. (e) Armstrong, F. A. *Curr. Opin. Chem. Biol.* **2004**, *8*, 133−140. (f) Frey, M. *ChemBioChem* **2002**, *3*, 153−160 and references therein..

(4) Cao, Z.; Hall, M. B. *J. Am. Chem. Soc.* **2001**, *123*, 3734−3742.

(5) (a) Liu, Z.-P.; Hu, P. *J. Am. Chem. Soc.* **2002**, *124*, 5175−5182. (b) Liu, Z.-P.; Hu, P. *J. Chem. Phys.* **2002**, *117*, 8177−8180.

(6) Parkin, A.; Cavazza, C.; Fontecilla-Camps, J. C.; Armstrong, F. A. *J. Am. Chem. Soc.* **2006**, *128*, 16808−16815.

(7) Greco, C.; Bruschi, M.; De Gioia, L.; Ryde, U. *Inorg. Chem.* **2007**, *46*, 5911−5921.

(8) Adamska, A.; Silakov, A.; Lambertz, C.; Rüdiger, O.; Happe, T.; Reijerse, E.; Lubitz, W. *Angew. Chem., Int. Ed.* **2012**, *51*, 11458−11462.

(9) Roseboom, W.; de Lacey, A. L.; Fernandez, V. M.; Hatchikian, C.; Albracht, S. P. J. *J. Biol. Inorg. Chem.* **2006**, *11*, 102−118.

(10) For recent reviews on models of the hydrogenases enzymes, see: (a) Simmons, T. R.; Berggren, G.; Bacchi, M.; Fontecave, M.; Artero, V. *Coord. Chem. Rev.* **2014**, *270*−*271*, 127−150. (b) Lubitz, W.; Ogata, H.; Rüdiger, O.; Reijerse, E. *Chem. Rev.* **2014**, *114*, 4081−4148. (c) Wang, N.; Wang, M.; Chen, L.; Sun, L. *Dalton Trans.* **2013**, *42*, 12059−12071. (d) Darensbourg, M. Y.; Weigand, W. *Eur. J. Inorg. Chem.* **2011**, 994−1004. (e) Tschierlei, S.; Ott, S.; Lomoth, R. *Energy Environ. Sci.* **2011**, *4*, 2340−2352. (f) Best, S. P.; Cheah, M. H. *Radiat. Phys. Chem.* **2010**, *79*, 185−194. (g) Gordon, J. C.; Kubas, G. J. *Organometallics* **2010**, *29*, 4682−4701. (h) Gloaguen, F.; Rauchfuss, T. B. *Chem. Soc. Rev.* **2009**, *38*, 100−108. (i) Capon, J.-F.; Gloaguen, F.; Pétillon, F. Y.; Schollhammer, P.; Talarmin, J. *Coord. Chem. Rev.* **2009**, *253*, 1476−1494. (j) Tard, C.; Pickett, C. J. *Chem. Rev.* **2009**, *109*, 2245−2274. (k) Felton, G. A. N.; Mebi, C. A.; Petro, B. J.; Vannucci, A. K.; Evans, D. H.; Glass, R. S.; Lichtenberger, D. L. *J. Organomet. Chem.* **2009**, *694*, 2681−2699. (l) Heinekey, D. M. *J. Organomet. Chem.* **2009**, *694*, 2671−2680. (m) Capon, J.-F.; Gloaguen, F.; Pétillon, F. Y.; Schollhammer, P.; Talarmin, J. *Eur. J. Inorg. Chem.* **2008**, 4671−4681.

(11) Munery, S.; Capon, J.-F.; De Gioia, L.; Elleouet, C.; Greco, C.; Pétillon, F. Y.; Schollhammer, P.; Talarmin, J.; Zampella, G. *Chem.—Eur. J.* **2013**, *19*, 15458−15461.

(12) Wang, W.; Rauchfuss, T. B.; Moore, C. E.; Rheingold, A. L.; De Gioia, L.; Zampella, G. *Chem.—Eur. J.* **2013**, *19*, 15476−15479.

(13) Jablonskyte, A.; Wright, J. A.; Fairhurst, S. A.; Webster, L. R.; Pickett, C. J. *Angew. Chem., Int. Ed.* **2014**, *53*, 10143−10146.

(14) Carroll, M. E.; Barton, B. E.; Rauchfuss, T. B.; Carroll, P. J. *J. Am. Chem. Soc.* **2012**, *134*, 18843−18852.

(15) (a) Camara, J. M.; Rauchfuss, T. B. *Nat. Chem.* **2012**, *4*, 26−30. (b) Camara, J. M.; Rauchfuss, T. B. *J. Am. Chem. Soc.* **2011**, *133*, 8098−8101.

(16) Razavet, M.; Borg, S. J.; George, S. J.; Best, S. P.; Fairhurst, S. A.; Pickett, C. J. *Chem. Commun.* **2002**, 700−701.

(17) (a) Hsieh, C.-H.; Erdem, O. F.; Harman, S. D.; Singleton, M. L.; Reijerse, E.; Lubitz, W.; Popescu, C. V.; Reibenspies, J. H.; Brothers, S. M.; Hall, M. B.; Darensbourg, M. Y. *J. Am. Chem. Soc.* **2012**, *134*, 13089−13102. (b) Singleton, M. L.; Bhuvanesh, N.; Reibenspies, J. H.; Darensbourg, M. Y. *Angew. Chem., Int. Ed.* **2008**, *47*, 9492−9495. (c) Thomas, C. M.; Liu, T.; Hall, M. B.; Darensbourg, M. Y. *Inorg. Chem.* **2008**, *47*, 7009−7024. (d) Thomas, C. M.; Darensbourg, M. Y.; Hall, M. B. *J. Inorg. Biochem.* **2007**, *101*, 1752−1757. (e) Liu, T.; Darensbourg, M. Y. *J. Am. Chem. Soc.* **2007**, *129*, 7008−7009.

(18) (a) Justice, A. K.; Nilges, M. J.; Rauchfuss, T. B.; Wilson, S. R.; De Gioia, L.; Zampella, G. *J. Am. Chem. Soc.* **2008**, *130*, 5293−5301. (b) Justice, A. K.; De Gioia, L.; Nilges, M. J.; Rauchfuss, T. B.; Wilson, S. R.; Zampella, G. *Inorg. Chem.* **2008**, *47*, 7405−7414. (c) Justice, A. K.; Rauchfuss, T. B.; Wilson, S. R. *Angew. Chem., Int. Ed.* **2007**, *46*, 6152−6154.

(19) It has now been established that the X bridgehead atom of the H cluster is an amine (NH) functional group,[19a−d] as proposed early on by Fontecilla-Camps and co-workers.[19e] (a) Silakov, A.; Wenk, B.; Reijerse, E.; Lubitz, W. *Phys. Chem. Chem. Phys.* **2009**, *11*, 6592−6599.

(b) Erdem, O. F.; Schwartz, L.; Stein, M.; Silakov, A.; Kaur-Ghumaan, S.; Huang, P.; Ott, S.; Reijerse, E. J.; Lubitz, W. *Angew. Chem., Int. Ed.* **2011**, *50*, 1439−1443. (c) Berggren, G.; Adamska, A.; Lambertz, C.; Simmons, T. R.; Esselborn, J.; Atta, M.; Gambarelli, S.; Mouesca, J.-M.; Reijerse, E.; Lubitz, W.; Happe, T.; Artero, V.; Fontecave, M. *Nature* **2013**, *499*, 66−69. (d) Esselborn, J.; Lambertz, C.; Adamska-Venkatesh, A.; Simmons, T.; Berggren, G.; Noth, J.; Siebel, J.; Hemschemeier, A.; Artero, V.; Reijerse, E.; Fontecave, M.; Lubitz, W.; Happe, T. *Nat. Chem. Biol.* **2013**, *9*, 607−609. (e) Nicolet, Y.; de Lacey, A. L.; Vernède, X.; Fernandez, V. M.; Hatchikian, E. C.; Fontecilla-Camps, J. C. *J. Am. Chem. Soc.* **2001**, *123*, 1596−1601.

(20) (a) Justice, A. K.; Zampella, G.; De Gioia, L.; Rauchfuss, T. B.; van der Vlugt, J. I.; Wilson, S. R. *Inorg. Chem.* **2007**, *46*, 1655−1664. (b) van der Vlugt, J. I.; Rauchfuss, T. B.; Wilson, S. R. *Chem.—Eur. J.* **2006**, *12*, 90−98. (c) van der Vlugt, J. I.; Rauchfuss, T. B.; Whaley, C. M.; Wilson, S. R. *J. Am. Chem. Soc.* **2005**, *127*, 16012−16013. (d) Boyke, C. A.; van der Vlugt, J. I.; Rauchfuss, T. B.; Wilson, S. R.; Zampella, G.; De Gioia, L. *J. Am. Chem. Soc.* **2005**, *127*, 11010−11018. (e) Boyke, C. A.; Rauchfuss, T. B.; Wilson, S. R.; Rohmer, M.-M.; Bénard, M. *J. Am. Chem. Soc.* **2004**, *126*, 15151−15160. (f) Lawrence, J. D.; Rauchfuss, T. B.; Wilson, S. R. *Inorg. Chem.* **2002**, *41*, 6193−6195.

(21) Huang, Y.; Gao, W.; Åkermark, T.; Li, M.; Åkermark, B. *Eur. J. Inorg. Chem.* **2012**, 4259−4263.

(22) Zheng, D.; Wang, M.; Chen, L.; Wang, N.; Cheng, M.; Sun, L. *Chem. Commun.* **2014**, *50*, 9255−9258.

(23) Dey, S.; Rana, A.; Crouthers, D.; Mondal, B.; Das, P. K.; Darensbourg, M. Y.; Dey, A. *J. Am. Chem. Soc.* **2014**, *136*, 8847−8850.

(24) Chouffai, D.; Zampella, G.; Capon, J.-F.; De Gioia, L.; Le Goff, A.; Pétillon, F. Y.; Schollhammer, P.; Talarmin, J. *Organometallics* **2012**, *31*, 1082−1091.

(25) The parameters i_p and E_p are respectively the peak current and the peak potential of a redox process; $E_{1/2} = (E_p^a + E_p^c)/2$; E_p^a, i_p^a and E_p^c, i_p^c are respectively the potential and the current of the anodic and of the cathodic peak of a reversible process; $\Delta E_p = E_p^a - E_p^c$. CV stands for cyclic voltammetry; v (V s^{-1}) is the scan rate in CV experiments. An ECE process consists of a chemical reaction (C) comprised between two electron transfer steps (E).

(26) (a) Bard, A. J.; Faulkner, L. R. *Electrochemical Methods: Fundamentals and Applications*; Wiley: New York, 1980. (b) Savéant, J.-M. *Elements of Molecular and Biomolecular Electrochemistry: An Electrochemical Approach to Electron Transfer Chemistry*; Wiley: New York, 2006.

(27) Chouffai, D.; Zampella, G.; Capon, J.-F.; De Gioia, L.; Gloaguen, F.; Pétillon, F. Y.; Schollhammer, P.; Talarmin, J. *Inorg. Chem.* **2011**, *50*, 12575−12585.

(28) (a) Gaudiello, J. G.; Wright, T. C.; Jones, R. A.; Bard, A. J. *J. Am. Chem. Soc.* **1985**, *107*, 888−897. (b) Moulton, R. D.; Chandler, D. J.; Arif, A. M.; Jones, R. A.; Bard, A. J. *J. Am. Chem. Soc.* **1988**, *110*, 5714−5725.

(29) Kuchynka, D. J.; Kochi, J. K. *Inorg. Chem.* **1988**, *27*, 2574−2581.

(30) Fitch, A.; Edens, G. J. *J. Electroanal. Chem.* **1989**, *267*, 1−13.

(31) Boehm, A.; Meerholz, K.; Heinze, J.; Muellen, K. *J. Am. Chem. Soc.* **1992**, *114*, 688−699.

(32) Koide, Y.; Schauer, C. K. *Organometallics* **1993**, *12*, 4854−4862.

(33) Eichhom, E.; Speiser, B. *J. Electroanal. Chem.* **1994**, *365*, 207−212.

(34) Edens, G. J.; Fitch, A.; Lavy-Feder, A. *J. Electroanal. Chem.* **1994**, *365*, 207−212.

(35) Digital CV simulations were done using DigiElch Special Build Version 3, see http://www.elchsoft.com and the following publications: (a) Rudolph, M. *J. Electroanal. Chem.* **2003**, *543*, 23−29. (b) Rudolph, M. *J. Electroanal. Chem.* **2004**, *571*, 289−307. (c) Rudolph, M. *J. Comput. Chem.* **2005**, *26*, 619−632. (d) Rudolph, M. *J. Comput. Chem.* **2005**, *26*, 633−641. (e) Rudolph, M. *J. Comput. Chem.* **2005**, *26*, 1193−1204.

(36) The introduction of supplementary reactions, namely, the disproportionation of cationic species $\mathbf{1P}^+$ and $\mathbf{1P'}^+$ transiently generated during the redox processes, was not successful in improving the fit between the experimental and the simulated CV data.

(37) The terms rotated and inverted refer to the iron-coordination geometry encountered in the crystal structures of the hydrogenase's active sites and the active sites of the Fe(II)Fe(I) redox states in the synthesized analogues. The vast majority of all of the other cases features a so-called eclipsed configuration of the two pyramidal geometries. To date, only two Fe(I)Fe(I) complexes were shown to adopt a rotated configuration in the solid state.[11,12]

(38) Roy, L. E.; Batista, E. R.; Hay, P. J. *Inorg. Chem.* **2008**, *47*, 9228−9237.

(39) Roy, L. E.; Jakubikova, E.; Graham Guthrie, M.; Batista, E. R. *J. Phys. Chem. A* **2009**, *113*, 6745−6750.

(40) Solis, B. H.; Hammes-Schiffer, S. *Inorg. Chem.* **2014**, *53*, 6427−6443.

(41) (a) Bhattacharjee, A.; Chavarot-Kerlidou, M.; Andreiadis, E. S.; Fontecave, M.; Field, M. J.; Artero, V. *Inorg. Chem.* **2012**, *51*, 7087−7093. (b) Fourmond, V.; Canaguier, S.; Golly, B.; Field, M. J.; Fontecave, M.; Artero, V. *Energy Environ. Sci.* **2011**, *4*, 2417−2427.

(42) Olsen, M. T.; Rauchfuss, T. B.; Wilson, S. R. *J. Am. Chem. Soc.* **2010**, *132*, 17733−17740.

(43) Zheng, D.; Wang, M.; Chen, L.; Wang, N.; Sun, L. *Inorg. Chem.* **2014**, *53*, 1555−1561.

(44) Zheng, D.; Wang, N.; Wang, M.; Ding, S.; Ma, C.; Darensbourg, M. Y.; Hall, M. B.; Sun, L. *J. Am. Chem. Soc.* **2014**, *136*, 16817−16823.

(45) Du Bois, D. L. *Inorg. Chem.* **2014**, *53*, 3935−3960.

(46) Morvan, D.; Capon, J.-F.; Gloaguen, F.; Le Goff, A.; Marchivie, M.; Michaud, F.; Schollhammer, P.; Talarmin, J.; Yaouanc, J.-J.; Pichon, R.; Kervarec, N. *Organometallics* **2007**, *26*, 2042−2052.

(47) (a) Becke, A. D. *Phys. Rev. A* **1988**, *38*, 3098−3100. (b) Perdew, J. P. *Phys. Rev. B* **1986**, *33*, 8822−8824.

(48) Schäfer, A.; Huber, C.; Ahlrichs, R. *J. Chem. Phys.* **1994**, *100*, 5829−5835.

(49) Ahlrichs, R.; Bar, M.; Haser, M.; Horn, H.; Kolmel, C. *Chem. Phys. Lett.* **1989**, *162*, 165−169.

(50) Eichkorn, K.; Weigend, F.; Treutler, O.; Ahlrichs, R. *Theor. Chem. Acc.* **1997**, *97*, 119−124.

(51) Jensen, F. *Introduction to Computational Chemistry*; John Wiley & Sons: Chichester, U.K., 2007.

(52) (a) Klamt, A. *J. Phys. Chem.* **1995**, *99*, 2224−2235. (b) Klamt, A. *J. Phys. Chem.* **1996**, *100*, 3349−3353.

(53) (a) Reiss, H.; Heller, A. *J. Phys. Chem.* **1985**, *89*, 4207−4213. (b) Harris, D. C. *Quantitative Chemical Analysis*; W. H. Freeman & Company: New York, 1987.

(54) (a) Pavlishchuk, V. V.; Addison, A. W. *Inorg. Chim. Acta* **2000**, *298*, 97−102. (b) Namazian, M.; Coote, M. L. *J. Phys. Chem. A* **2007**, *111*, 7227−7232.

(55) Izutsu, K. *Electrochemistry in Nonaqueous Solutions*; Wiley-VCH: New York, 2002.